Electronic Supplementary Information (ESI)

N-doping of nonfullerene bulk-heterojunction organic solar cells strengthens photogeneration and exciton dissociation

Jiaqi Xie,[a] Weihua Lin,[b] Guillermo C. Bazan,[c] Tõnu Pullerits,[b] Kaibo Zheng,[b,d*] and Ziqi Liang[a*]

[*][a] Prof. Z. Liang, J. Xie
Department of Materials Science
Fudan University
Shanghai 200433, China
Email: zqliang@fudan.edu.cn

[b] Prof. T. Pullerits, K. Zheng, W. Lin
Department of Chemical Physics and NanoLund
Lund University, Box 124, 22100
Lund, Sweden

[c] Prof. G. C. Bazan
Department of Chemistry
National University of Singapore
Singapore 117543, Singapore

[*][d] Prof. K. Zheng
Department of Chemistry
Technical University of Denmark
DK-2800 Kongens Lyngby, Denmark
Email: kzheng@kemi.dtu.dk

Experimental Section

Materials: PM6 and Y6 were purchased from Derthon Optoelectronics Materials Science Technology Co. Ltd. (China). *N*-DMBI was purchased from purchased from Sigma-Aldrich. All materials were used as received without further purification.

Solution and Thin Film Preparation: For PM6:Y6:*N*-DMBI blend and PM6/Y6:*N*-DMBI neat solutions, *N*-DMBI content (*x* wt%) was calculated as $x_{blend} = \frac{m_{N-\mathrm{DMBI}}}{m_{\mathrm{PM6}}+m_{\mathrm{Y6}}}$ and $x_{\mathrm{PM6\ or\ Y6}} = \frac{m_{N-\mathrm{DMBI}}}{m_{\mathrm{PM6\ or\ Y6}}}$, in which m_i denoted the mass to *N*-DMBI, PM6 and Y6. For neat solutions, the values of x_{PM6} and x_{Y6} can be converted into 2.2 x_{blend} and 1.8 x_{blend}, respectively, because of the PM6:Y6 weight ratio of 1:1.2. Specifically, if x_{blend} was 0.002, 0.005, 0.008, 0.015 and 5 wt%, then the corresponding x_{PM6} was 0.004, 0.011, 0.018, 0.033, 11 wt% and x_{Y6} was 0.003, 0.009,

0.014, 0.027, 9.167 wt%. Substrates were ultrasonically cleaned by detergent, deionized water, acetone and isopropyl alcohol in sequence for 20 min each step and then to be dried by nitrogen flow and treated by UV-ozone for 20 min. Chloroform (CF) solutions of 16.5 mg/mL PM6:Y6 (1:1.2 by weight), 10 mg/mL PM6 and 15 mg/mL Y6 with *N*-DMBI and 0.5 v/v chloronaphthalene (CN) were stirred at 50 °C for 2 h in N_2-filled glovebox before using. Chloroform solutions of PTB7-Th:ITIC (1:1.3), PTB7-Th:IT-4F (1:1.3) and PTB7-Th:IEICO-4F (1:1.5) were prepared in 25 mg/mL without any additives according to Lin' and Chen's work.[S1,S2] For UV-Vis, step profilometer and contact angle samples, solutions were rapidly spun onto a rotating glass substrate at 3000 rpm, and the condensed films were then annealed at 100 °C for 10 min in nitrogen-filled glovebox. For KPFM samples, same procedures were applied but using silicon substrate instead. For GIWAXS samples, solutions were drop-casted onto silicon substrate. For PL samples, solutions were diluted into 5 mg/mL.

Thin-film Characterization: Film thickness was determined by Bruker DektakXT step profilometer. EPR spectra were measured by Bruker EMXPLUS, and ^{1}HNMR spectra were acquired by MercuryPlus spectrometer in deuterated chloroform solution at room temperature. To thermally activate doping process, Y6/*N*-DMBI neat and Y6:*N*-DMBI blend solutions were sealed in bottles and heated at 100 °C for 2 min in glovebox before the testing. FT-IR spectra were acquired by beamline BL01B at Shanghai Synchrotron Radiation Facility (SSRF), and the powder samples were obtained by redrying the as-prepared solutions. Thin film thicknesses were measured by Alpha-Step D-500 stylus profilometer. KPFM images were captured by Bruker Dimension Icon in tapping mode, and the contact potential were resolved by the software of Nano Scope Analysis. GIWAXS patterns were acquired by beamline BL14B1 at SSRF with an X-ray source of 10 keV and incident angle of 0.2°, and the measured spectra were further corrected by a MATLAB toolbox of *GIXSGUI*.[S3] Contact angle images were

captured by Harke-SPCA, and the surface tension was determined by Owen-Wendt method. Absorbance spectra were measured by Agilent 8453 UV–Visible spectrometer. PL and TRPL spectra were measured by Spex Fluorolog 1681 spectrofluorometer, and PM6 and Y6 were excited at 532 and 687 nm, respectively. TAS were recorded by a femtosecond pump-probe setup in N_2 atmosphere, and samples were selectively excited by 800 or 400 nm lasers with 80 fs pulse length, then the charge generation process was analyzed by SVD method using Glotaran software package.

Device Fabrication and Measurement: ITO substrates (15 Ω/square) were cleaned following the same procedures as that for thin-film preparation above. OSCs were fabricated in inverted architecture of ITO/ZnO/active layer/MoO_3/Ag. The ZnO precursor solution was prepared by dissolving 200 mg zinc acetate dihydrate into 2 mL of 2-methoxyethanol and 60 μL of 2-aminoethanol and stirred at room temperature overnight. In air, ZnO precursor solution was spin-coated at 5000 rpm and annealed at 200 °C for 30 min. Then samples were transferred into glovebox, wherein active layer solutions were spun onto substrate at 3000 rpm and annealed at 100 °C for 10 min. Finally, samples were transferred into a thermal evaporator to sequentially deposit 10 nm MoO_3 and 120 nm Ag layers with electrode shadow mask. Light *J*–*V* curves were recorded by Keithley 2400 source meter under AM 1.5G irradiation (Newport-Oriel) with the intensity of 100 mW cm^{-2}. Stability test were performed for the non-encapsulated devices that are stored in N_2-filled glovebox, but the measurement were conducted in air following the same procedures as light *J*-*V* measurement. EQE profiles were measured by QE-R setup purchased from Enli Technology Co. Ltd with 500 W xenon lamp. MIM-CELIV was performed by an arbitrary function generator (Tektronix AFG3021C, 25MHz bandwidth) to provide a linearly increasing voltage pulse and an oscilloscope (DPO4104B, 1 GHz) to monitor the transient current. To estimate charge carrier mobility (μ) from the MIM-

CELIV measurement, a linear dependence between t_{max}^{-2} and V_{off} can be predicted by an equation of $t_{max}^{-2} = \frac{eA\mu}{k_B T d^2}\left(V_{bi} - V_{off}\right)$ for the condition of $V_{off} < V_{bi} - 4k_B T/e$, wherein t_{max} is, e is elementary charge, A is the active layer area of 0.04 cm^2, d is the active layer thickness of ~100 nm, k_B is Boltzmann constant, T is room temperature of 300 K. Upon plotting t_{max}^{-2} as a function of V_{off} as shown in Fig. 5g, V_{bi} is estimated from the intersection with the V_{off} axis of the extrapolated line, which is about 600, 580 and 590 mV for the devices with 0, 0.005 and 0.02 wt% *N*-DMBI, respectively.[S4]

Space-Charge Limited Current Measurement: Hole-only and electron-only devices were fabricated in the configurations of ITO/PEDOT:PSS/active layer/MoO_3/Ag and ITO/ZnO/active layer/PFN-Br/Ag, respectively. Their fabrications were similar to that of solar cells with the only difference in PEDOT:PSS and PFN-Br layers. Water solution of PEDOT:PSS was spin-coated onto ITO substrate at 3000 rpm and annealed at 150 °C for 20 min in air. 0.5 mg/mL methanol solution of PFN-Br was spun onto substrate at 3000 rpm and annealed at 100 °C for 10 min in glovebox. SCLC measurement was performed under dark condition, and a bias (V) was scanned from 0 to 8 V with a step of 0.02 V. Charge carrier mobility was determined according to Mott–Gurney Law, $J \times d = \frac{9}{8}\mu\varepsilon_r\varepsilon_0 E^2$, wherein ε_r is relative dielectric constant, ε_0 is vacuum permittivity, d is active layer thickness and E is electrical field equal to V/d.[S5]

Results

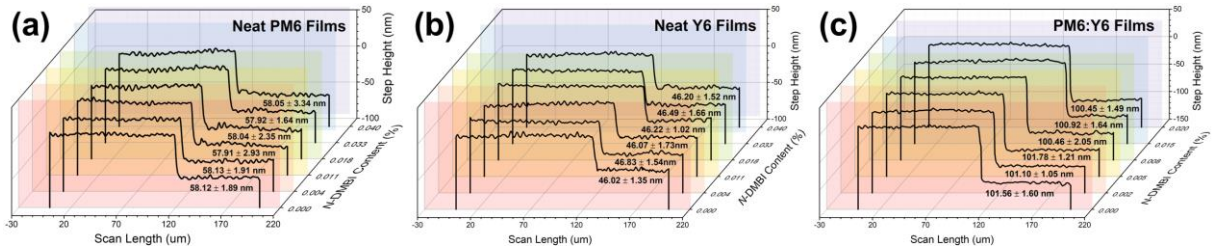

Fig. S1 Step profilometer measurement for the thickness of (a) neat PM6, (b) neat Y6 and (c) PM6:Y6 blend films that contain *x* wt% *N*-DMBI corresponding to the absorbance measurement shown in Fig. 1b.

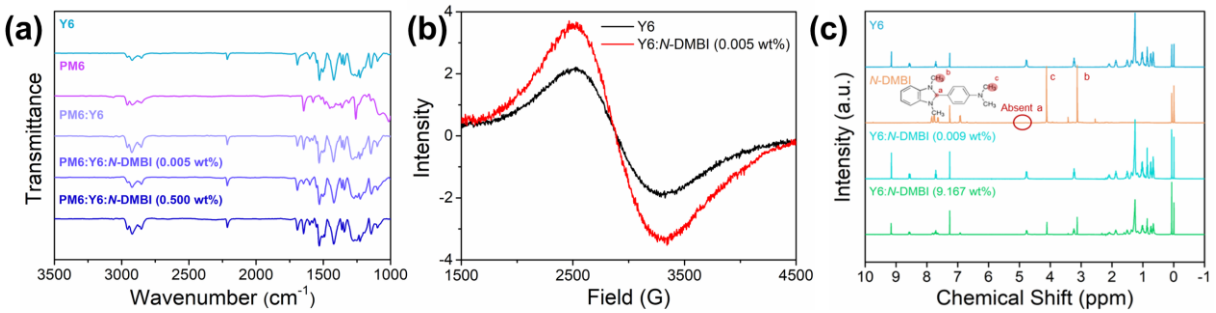

Fig. S2 (a) EPR spectra of neat Y6 and Y6:*N*-DMBI (0.005 wt%),(b)FT-IR spectra of Y6, PM6 and PM6:Y6:*N*-DMBI (*x* wt%) powders, and (c) ^{1}H-NMR spectra of Y6, *N*-DMBI and Y6:*N*-DMBI (*x* wt%) in $CDCl_3$ solution.

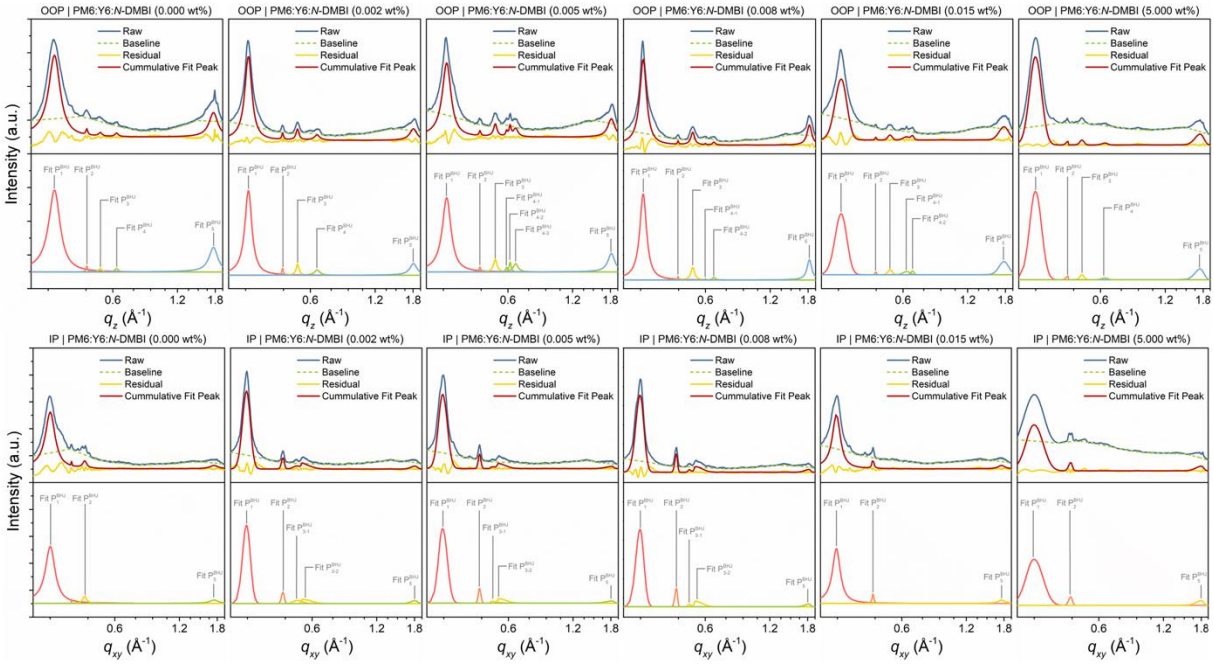

Fig. S3 Gauss and Lorentz peak fittings of the1D GIWAXS linecuts for the samples of PM6:Y6:*N*-DMBI (*x* wt%).

Table S1 Summary of lamellar and π–π stacking fitting results for the GIWAXS linecuts of PM6:Y6:*N*-DMBI (*x* wt%) as shown in Fig. S2

	OOP				IP			
***N*-DMBI (wt%)**	**Adj. R Square**	**Peak**	**Position**	**FWHM**	**Adj. R Square**	**Peak**	**Position**	**FWHM**
0.000	0.97532	P_1^{BHJ}	0.3211	0.0479	0.976135	P_1^{BHJ}	0.3005	0.0378
		P_5^{BHJ}	1.7655	0.2014		P_5^{BHJ}	1.7402	0.1904
0.002	0.98965	P_1^{BHJ}	0.3192	0.0283	0.98859	P_1^{BHJ}	0.2987	0.0297
		P_5^{BHJ}	1.8080	0.1702		P_5^{BHJ}	1.8102	0.1480
0.005	0.97318	P_1^{BHJ}	0.3111	0.0243	0.98859	P_1^{BHJ}	0.2948	0.0273
		P_5^{BHJ}	1.8201	0.1079		P_5^{BHJ}	1.8305	0.1299
0.008	0.983221	P_1^{BHJ}	0.3084	0.0268	0.990688	P_1^{BHJ}	0.2928	0.0279
		P_5^{BHJ}	1.8255	0.1121		P_5^{BHJ}	1.8240	0.1340
0.015	0.986227	P_1^{BHJ}	0.3059	0.0462	0.984092	P_1^{BHJ}	0.2914	0.0304
		P_5^{BHJ}	1.7717	0.2163		P_5^{BHJ}	1.7516	0.1514
5.000	0.998831	P_1^{BHJ}	0.2988	0.0454	0.995603	P_1^{BHJ}	0.2866	0.0648
		P_5^{BHJ}	1.7434	0.1947		P_5^{BHJ}	1.7169	0.1780

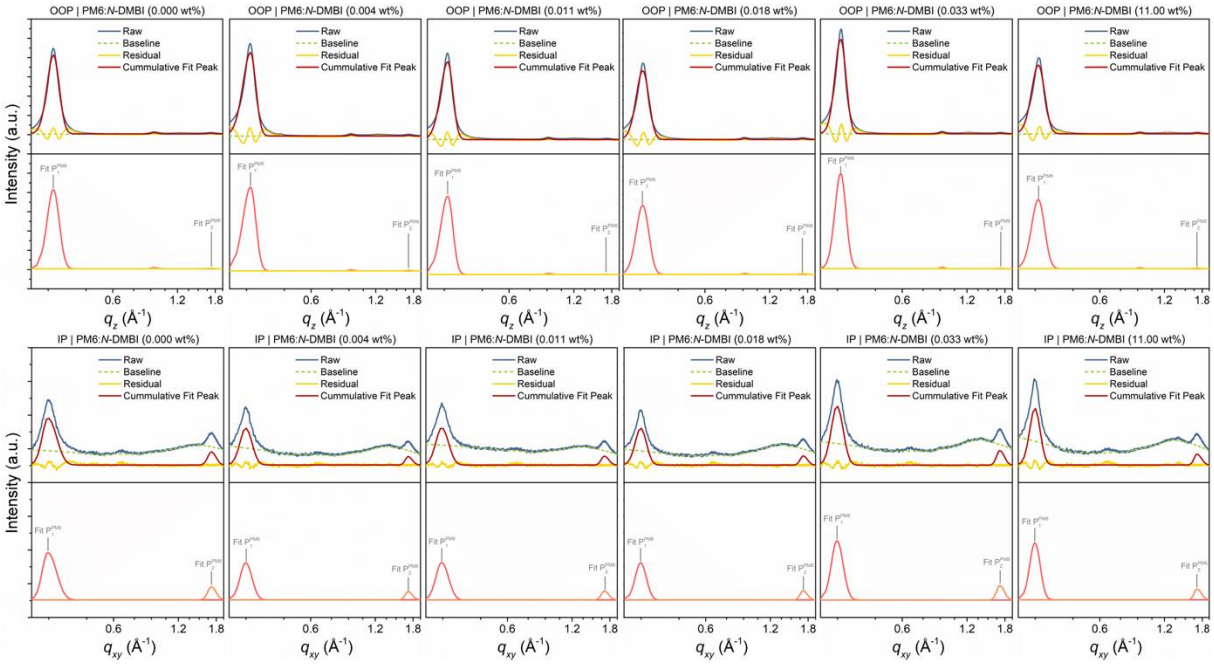

Fig. S4 Gauss and Lorentz peak fittings of the1D GIWAXS linecuts for the samples of PM6:*N*-DMBI (*x* wt%).

Table S2 Summary of lamellar and π–π stacking fitting results for the GIWAXS linecuts of PM6:*N*-DMBI (*x* wt%) as shown in Fig. S3

	OOP				IP			
***N*-DMBI (wt%)**	**Adj. R Square**	**Peak**	**Position**	**FWHM**	**Adj. R Square**	**Peak**	**Position**	**FWHM**
0.000	0.987955	P_1^{PM6}	0.3171	0.0509	0.982552	P_1^{PM6}	0.2968	0.0543
		P_2^{PM6}	1.7252	0.1220		P_2^{PM6}	1.7082	0.180
0.004	0.982504	P_1^{PM6}	0.3131	0.0485	0.977989	P_1^{PM6}	0.2987	0.0454
		P_2^{PM6}	1.7172	0.0966		P_2^{PM6}	1.7073	0.1540
0.011	0.983857	P_1^{PM6}	0.3107	0.0480	0.982361	P_1^{PM6}	0.2985	0.0450
		P_2^{PM6}	1.7009	0.0746		P_2^{PM6}	1.7072	0.1444
0.018	0.98095	P_1^{PM6}	0.3083	0.0492	0.973065	P_1^{PM6}	0.2984	0.0423
		P_2^{PM6}	1.7010	0.0837		P_2^{PM6}	1.7072	0.1572
0.033	0.980439	P_1^{PM6}	0.3079	0.0504	0.987165	P_1^{PM6}	0.2982	0.0447
		P_2^{PM6}	1.7023	0.0923		P_2^{PM6}	1.7034	0.1680
11.00	0.979541	P_1^{PM6}	0.3070	0.0511	0.978584	P_1^{PM6}	0.2988	0.0399
		P_2^{PM6}	1.6991	0.1072		P_2^{PM6}	1.6998	0.1735

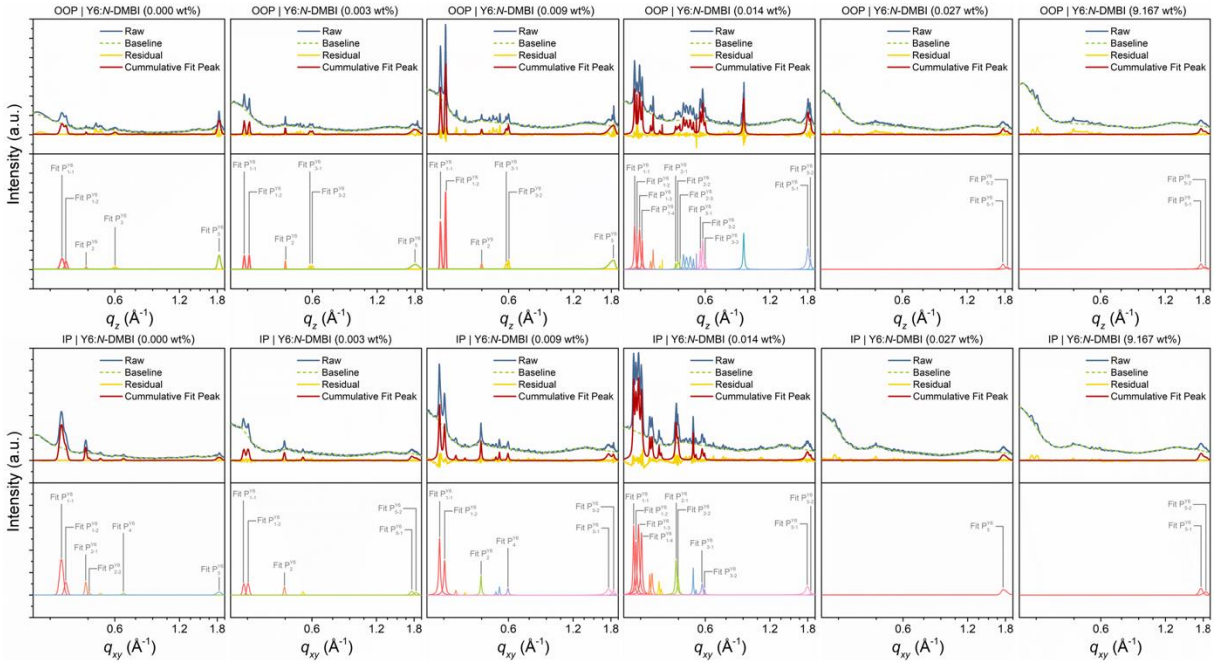

Fig. S5 Gauss and Lorentz peak fittings of the1D GIWAXS linecuts for the samples of Y6:*N*-DMBI (*x* wt%).

Table S3 Summary of lamellar and π–π stacking fitting results for the GIWAXS linecuts of Y6:*N*-DMBI (*x* wt%) as shown in Figure S4

	OOP				IP			
***N*-DMBI (wt%)**	**Adj. R Square**	**Peak**	**Position**	**FWHM**	**Adj. R Square**	**Peak**	**Position**	**FWHM**
0.000	0.87266	P_{1-1}^{Y6}	0.3408	0.0257	0.991007	P_{1-1}^{Y6}	0.3386	0.0297
		P_{5}^{Y6}	1.8044	0.0679		P_{5}^{Y6}	1.8151	0.1617
0.003	0.861185	P_{1-1}^{Y6}	0.2896	0.0104	0.898747	P_{1-1}^{Y6}	0.2885	0.0179
		P_{5}^{Y6}	1.8283	0.0587		P_{5}^{Y6}	1.8368	0.1635
0.009	0.914463	P_{1-1}^{Y6}	0.2889	0.0091	0.957434	P_{1-1}^{Y6}	0.2865	0.0116
		P_{5}^{Y6}	1.8454	0.0554		P_{5}^{Y6}	1.8498	0.1418
0.014	0.951805	P_{1-1}^{Y6}	0.2813	0.0130	0.976852	P_{1-1}^{Y6}	0.2783	0.0216
		P_{5-2}^{Y6}	1.8052	0.0822		P_{5-2}^{Y6}	1.8363	0.1040
0.027	0.864329	/	/	/	0.863270	/	/	/
		P_{5-2}^{Y6}	1.7630	3.5639		P_{2}^{Y6}	1.7561	0.1219
9.167	0.861017	/	/	/	0.948533	/	/	/
		P_{5-2}^{Y6}	1.7573	3.5755		P_{5-2}^{Y6}	1.7555	0.1898

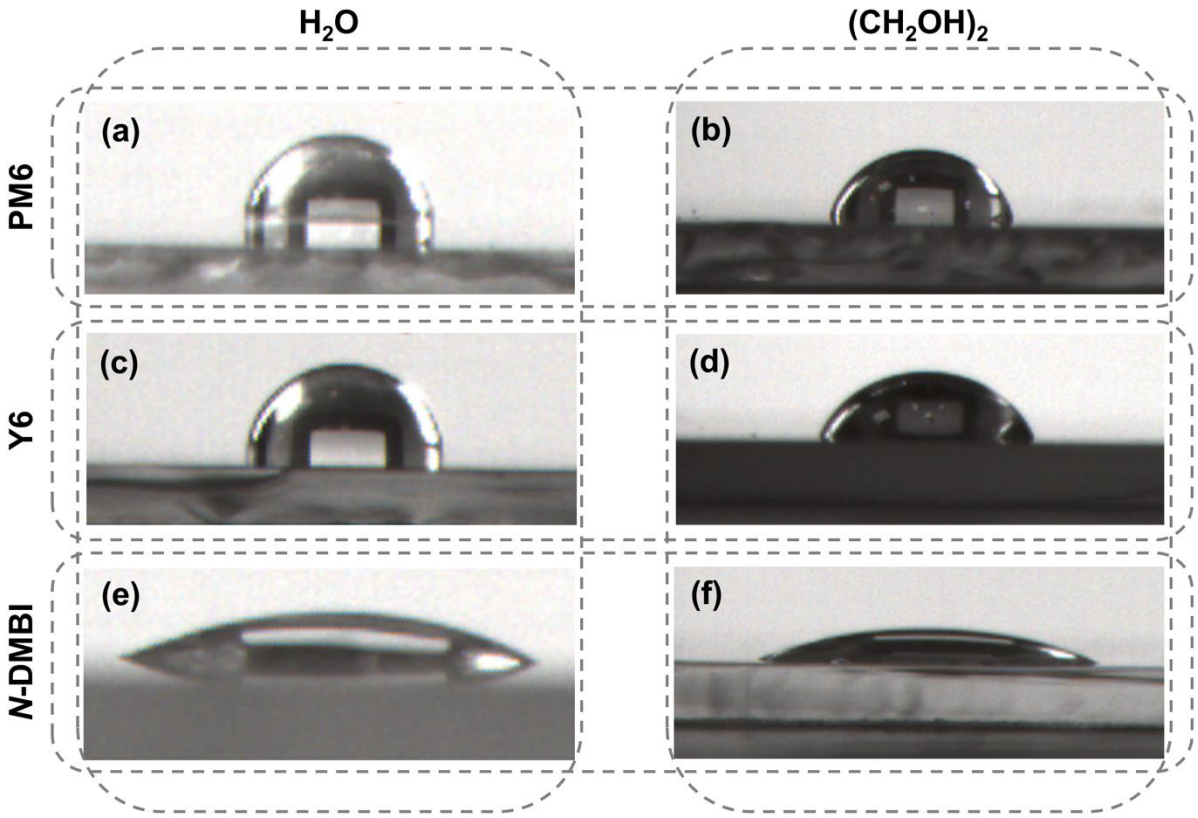

Fig. S6 Contact angle images of (a,b) PM6, (c,d) Y6 and (e,f) *N*-DMBI with a droplet of water (H_2O) or ethylene glycol ($(CH_2OH)_2$) on the surface.

Table S4 List of the known surface energy of H_2O and $(CH_2OH)_2$, and the corresponding polar and dispersion part[S6]

	γ_{LV} (mN/m)	γ_{LV}^{d} (mN/m)	γ_{LV}^{p} (mN/m)
H_2O	72.8	22.1	50.7
$(CH_2OH)_2$	48.3	29.3	19.0

Table S5 H_2O and $(CH_2OH)_2$ contact angles on PM6, Y6 and *N*-DMBI films. The free surface energy (γ) is calculated by the equations of $\gamma_{LV}(1+cos\theta) = 2\sqrt{\gamma_{SV}^{d}\gamma_{LV}^{d}} + 2\sqrt{\gamma_{SV}^{p}\gamma_{LV}^{p}}$ and $\gamma_{SV} = \gamma_{SV}^{d} + \gamma_{SV}^{p}$, where the superscripts of *d* and *p* denote the dispersion and polar part, and the subscripts of *SV* and *LV* denote the solid-vapor and liquid-vapor, respectively[S6]

	H_2O Angle	$(CH_2OH)_2$ Angle	γ_{LV}^{d} (mN m^{-1})	γ_{LV}^{p} (mN m^{-1})	γ_{SV} (mN m^{-1})
PM6	99.4°	76.0°	20.04	1.75	21.79
Y6	98.4°	71.0°	26.23	0.97	27.20
N-DMBI	28.5°	21.1°	6.42	62.92	69.34

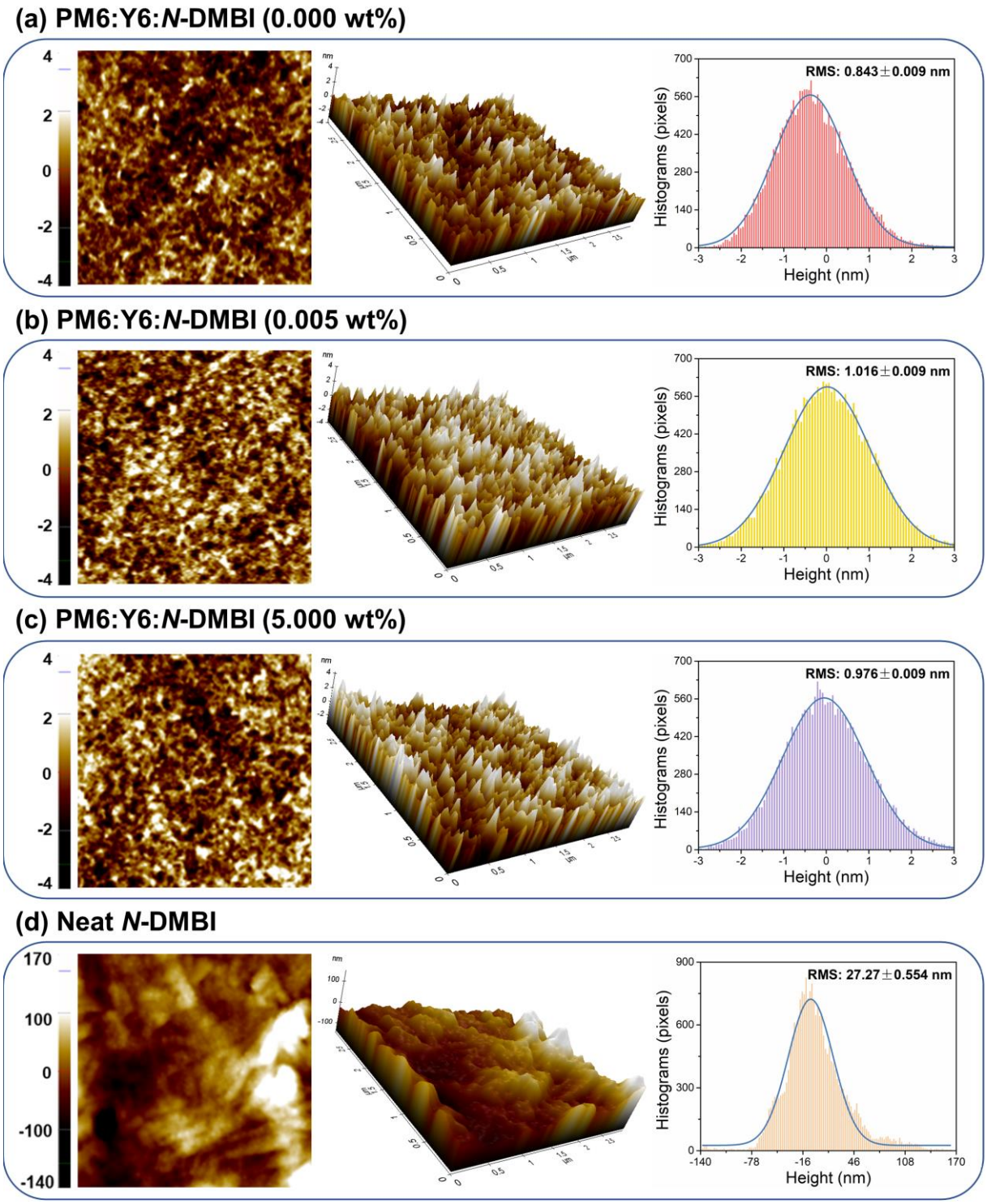

Fig. S7 Planar, 3D and the measured height histograms of AFM images for 3 μm ×3 μm photoactive layers of (a) PM6:Y6:*N*-DMBI (0 wt%), (b) PM6:Y6:*N*-DMBI (0.005 wt%) and PM6:Y6:*N*-DMBI (5 wt%).

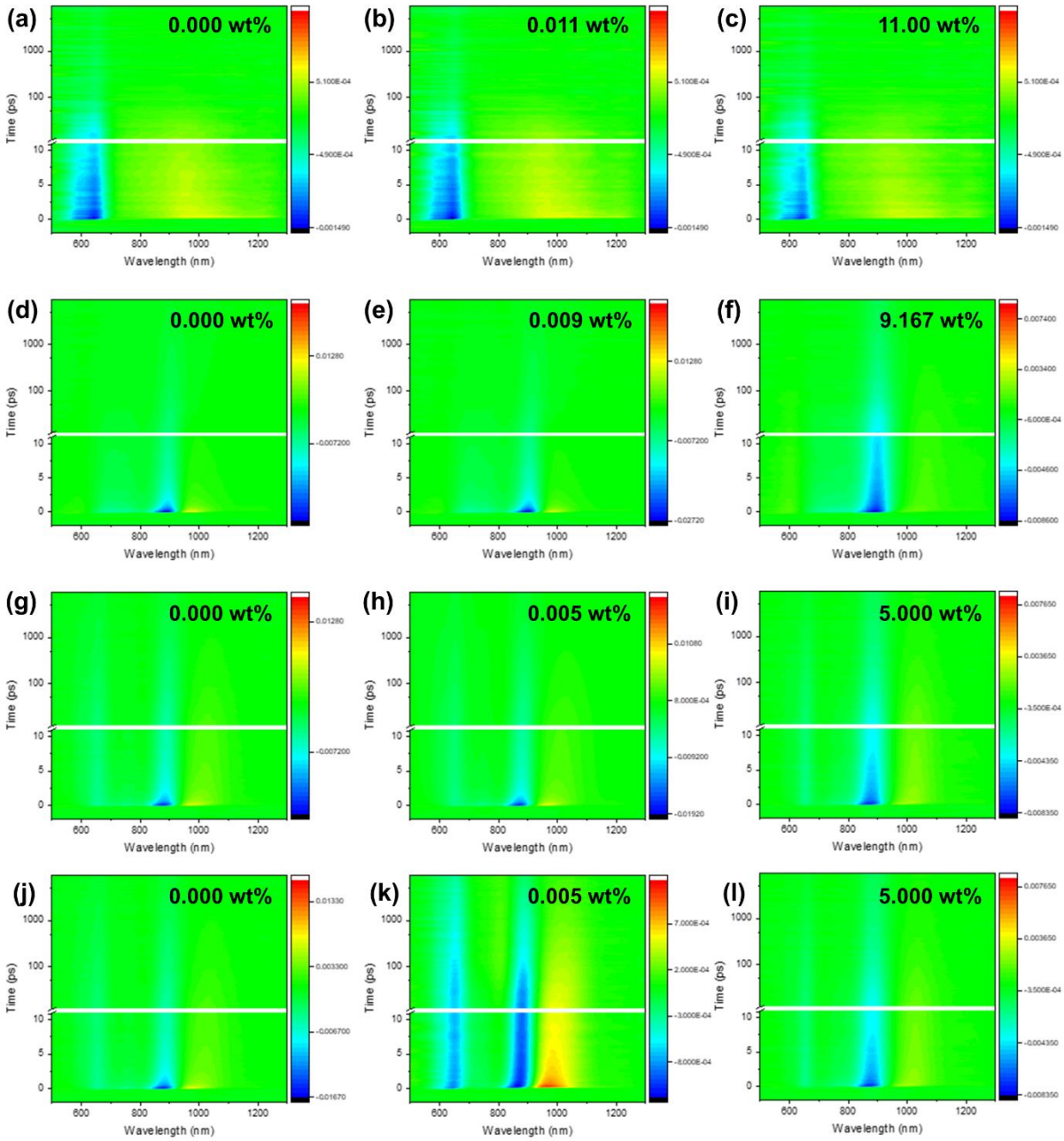

Fig. S8 TAS profiles of (a–c) PM6:*N*-DMBI (*x* wt%), (d–f) Y6: *N*-DMBI (*x* wt%) and (j–l) PM6:Y6:*N*-DMBI (*x* wt%).

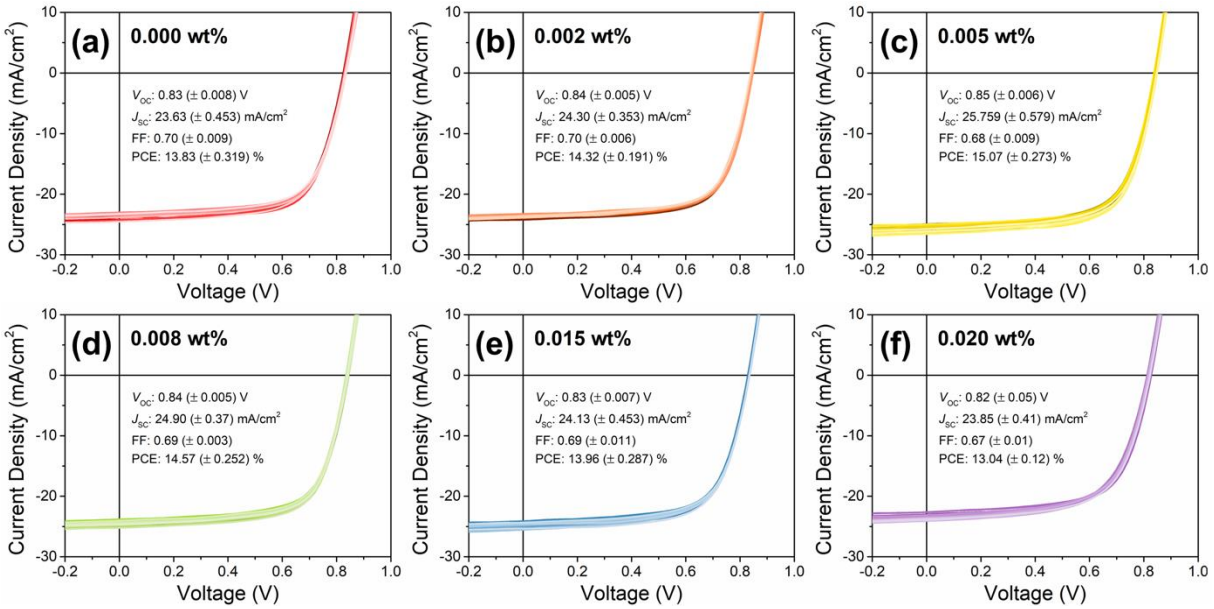

Fig. S9 (a–f) *J*-*V* curves of 20 devices as a function of *N*-DMBI content with the average V_{OC}, J_{SC}, FF and PCE values.

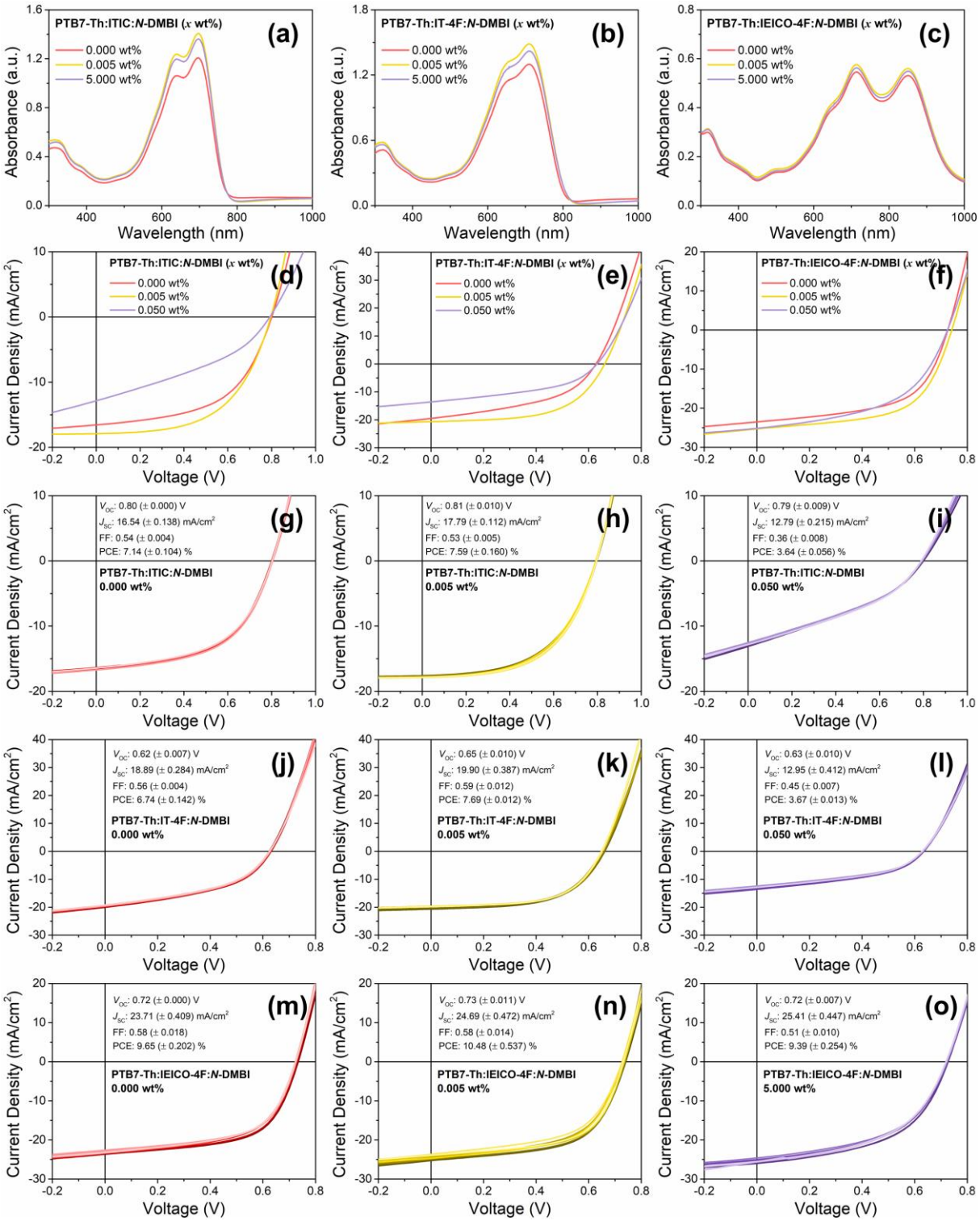

Fig. S10 Optical and photovoltaic performance of other NFA-based light-harvesting layers with 0, 0.005 and 0.05 wt% *N*-DMBI inclusions. UV-vis absorption spectroscopy of (a) PTB7-ITIC:*N*-DMBI (*x* wt%), (b) PTB7-Th:IT-4F (*x* wt%), and (c) PTB7-Th:IEICO-4F (*x* wt%) blend films. (d–f) The *J-V* curves of the best-performing devices for each D:A combinations, and the extracted photovoltaic parameters are listed in Table S6. The *J-V* curves of 8 devices as a function of *N*-DMBI content with the average V_{OC}, J_{SC}, FF and PCE values for the corresponding (g–i) PTB7-Th:ITIC, (j–l) PTB7-Th:IT-4F and (m–o) PTB7-Th:IEICO-4F blends.

Table S6 Summary of the photovoltaic parameters of the best-performing inverted OSCs with the active layers consisting of PTB7-Th:ITIC:*N*-DMBI, PTB7-Th:IT-4F:*N*-DMBI and PTB7-Th:IEICO-4F:*N*-DMBI blends as shown in Fig. S13.

	***N*-DMBI (wt%)**	**V_{OC} (V)**	**J_{SC} (mA/cm^2)**	**FF**	**PCE (%)**
PTB7-Th:ITIC	0.000	0.80	16.73	0.54	7.28
	0.005	0.82	17.91	0.53	7.80
	0.050	0.80	12.86	0.36	3.73
PTB7-Th:IT-4F	0.000	0.62	19.57	0.56	6.82
	0.005	0.66	20.67	0.57	7.84
	0.050	0.64	13.60	0.44	3.85
PTB7-Th:IEICO-4F	0.000	0.72	24.18	0.58	9.84
	0.005	0.74	25.28	0.59	11.05
	0.050	0.72	26.01	0.52	9.81

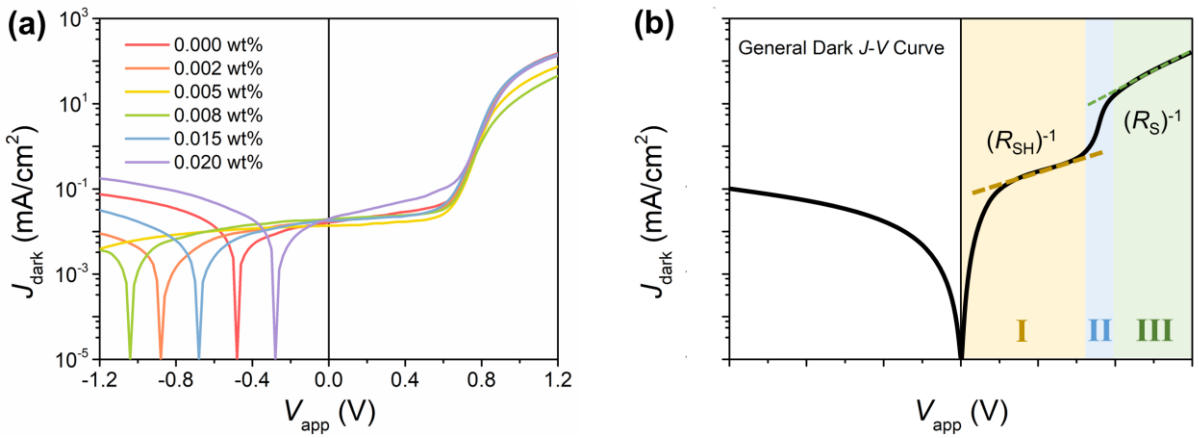

Fig. S11 (a) Dark *J-V* curves of the best-performing solar cells that contain varied amount of *N*-DMBI dopant, and (b) illustration of deriving the cell R_{SH} and R_S from the slopes of a general dark *J-V* curve.

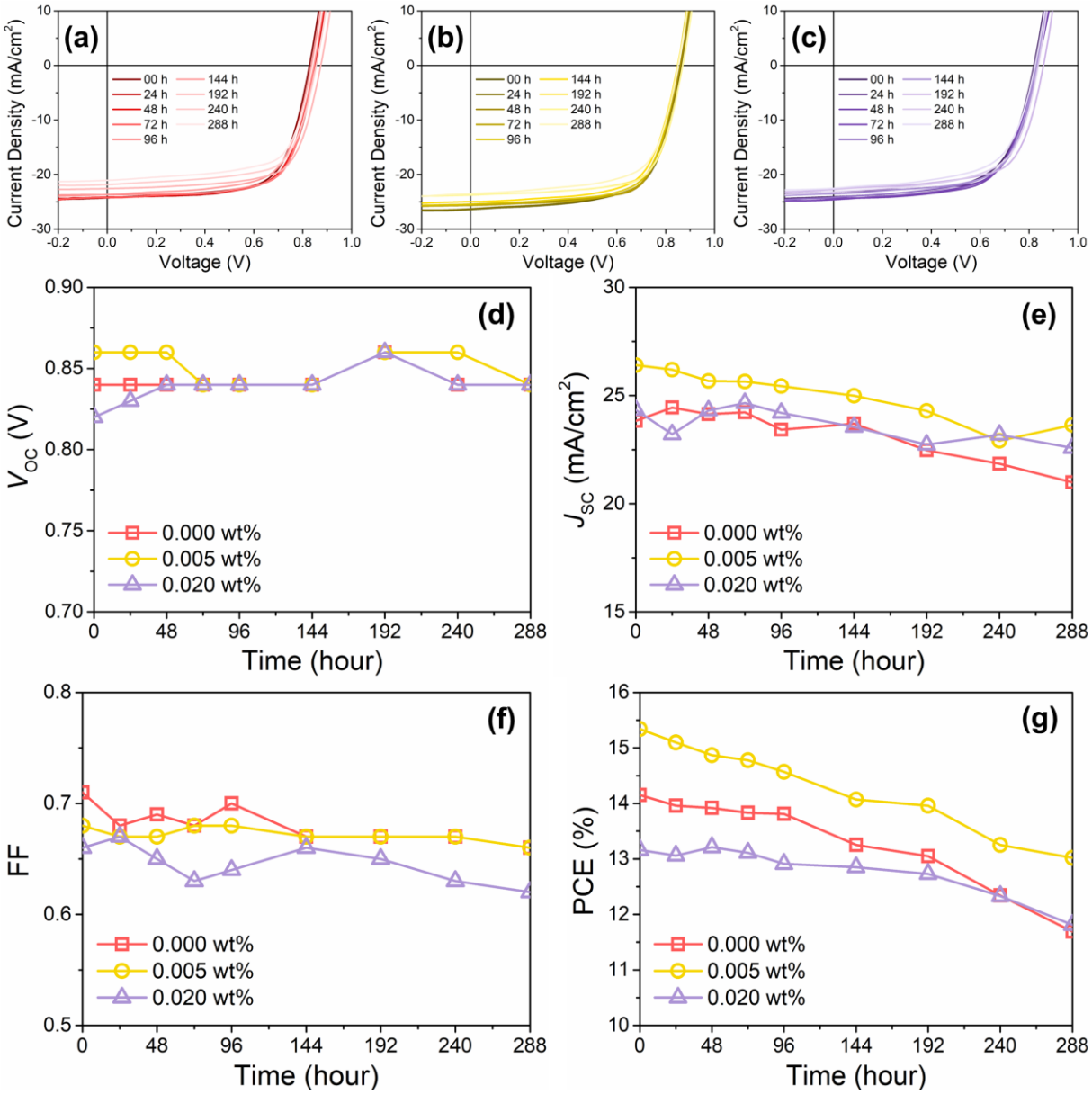

Fig. S12 Evolutions of the PM6:Y6:*N*-DMBI (x wt%) based photovoltaic performance in 288 hours. (a–c) *J*-*V* curves of the best-performing devices that contain 0, 0.005 and 0.02 wt% *N*-DMBI at each time point. Corresponding (d) V_{OC}, (e) J_{SC}, (f) FF and (g) PCE changes that are extracted from the *J*-*V* curves in (a–c).

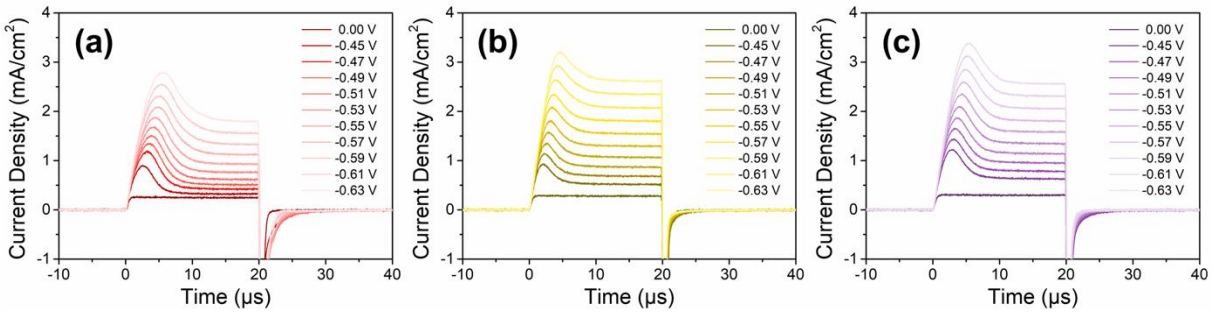

Fig. S13 MIM-CELIV measurement of the best-performed solar cells that contain (a) 0, (b) 0.005 and (c) 0.02 wt% *N*-DMBI dopant.

References

S1 Y. Lin, J. Wang, Z. Zhang, H. Bai, Y. Li, D. Zhu, X. Zhan, *Adv. Mater.* **2015**, *27*, 1170–1174.

S2 M. Chen, D. Liu, W. Li, R. S. Gurney, D. Li, J. Cai, E. L. K. Spooner, R. C. Kilbride, J. D. McGettrick, T. M. Watson, Z. Li, R. A. L. Jones, D. G. Lidzey, T. Wang, *ACS Appl. Mater. Interfaces*, 2019, 11, 26194-26203.

S3 Z. Jiang, *J. Appl. Cryst.* **2015**, *48*, 917.

S4 R. Hanfland, M. A. Fischer, W. Brütting, U. Würfel, R. C. I. MacKenzie, *Appl. Phys. Lett.* **2013**, *103*, 063904.

S5 Y. Yan, Y. Yang, M. Liang, M. Abdellah, T. Pullerits, K. Zheng, Z. Liang, *Nat. Commun.* **2021**, *12*, 6603.

S6 H. Chen, R. Zhang, X. Chen, G. Zeng, L. Kobera, S. Abbrent, B. Zhang, W. Chen, G. Xu, J. Oh, S.-H. Kang, S. Chen, C. Yang, J. Brus, J. Hou, F. Gao, Y. Li, Y. Li, *Nat. Energy* **2021**, *6*, 1045.